Synthesis, Characterization and Catalytic application of Mn-MFI prepared by different methods

MOHAMED SAYED THABET

Chemistry Department, College of Science, Jazan University, Jazan,45142, Saudi Arabia.
*Corresponding author E-mail: mthabet@jazanu.edu.sa

ABSTRACT

Utilizing various techniques, the synthesis of silicalite-1 (MFI), Mn-MFI$_{in\text{-}situ}$, and Mn-MFI$_{Imp}$ samples derived from rice husk has been studied. Several physico-chemical approaches were used to characterize the produced materials. The results showed that the addition of Mn ions through in-situ preparation methods will result in a rearrangement of Silicalite's structural composition and disappearance of quartz silica. The presence of crystalline MnO_2 species was noted in Mn-MFI$_{in\text{-}situ}$, dealumination, and a decrease in cell volume. According to XRD, ESR, and surface texture analyses, all of the samples' FTIR spectra showed MFI structure and good assimilation of Mn species into MFI channels. The catalytic activity of the samples was measured and judged to be toward hydroxylation of benzene at a temperature of 80 degrees Celsius. The data revealed that the catalytic activity occurred in the following order: Silicalite > Mn-MFI$_{imp}$ > Mn-MFI$_{in\text{-}situ}$.

Keywords: Rice husk, Silicalite, Zeolite, Catalytic activity, Hydroxylation.

INTRODUCTION

In the fields of fibers, resins, plasticizers, agrochemicals, antioxidants, and medications, phenol is a crucial chemical. The direct hydroxylation of benzene is extremely interesting from the point of view for both scientific and industrial perspectives[1–3]. Due to the challenges of direct hydroxylation of energetically stable benzene and production of a ketone as a byproduct in commonly used cumene methods, the one-step hydroxylation of benzene to phenol is a complex reaction. As a result, there is a lot of work being done to create a novel method for benzene oxidation that can be used to synthesize phenol[4,5].

Various researches used silica-based molecular sieves as catalysts in a variety of industrial applications from the refinement of crude oil to the fabrication of intermediates and cosmetic chemicals and exhibit extraordinary catalytic capabilities[6,7].

A molecular sieve made of microporous silicon called Silicalite-1 has a tetrahedral MFI structure[8,9]. It has been noted that new molecular sieves with selective oxidation capabilities can be produced by isomorphous substituting Silicon (vi) ions in framework of silicalite-1 with tetra- and pentavalent ions like Titanium, Vanadium or Tin[10,11]. It has been demonstrated that the silica minerals Ti, V and Sn silicalite-1 have special catalytic

capabilities in oxidation reactions using H_2O_2 as the oxidant[12,13].

There have been reports of the production of high-quality inorganic membranes for catalytic membrane reactors using isomorphous substituting the trivalent ions Al^{3+}, B^{3+}, Fe^{3+}, and Ge^{3+} for the Si^{4+} ions in silicalite-1[14,15]. The high-silica aluminosilicate molecular sieve (zeolites) known as aluminum-containing silicalite-1 (ZSM-5) exhibits significant importance as catalytic materials For the inclusion of manganese into silicalite-1, two synthetic techniques have been described[16,17] recrystallizing Mn(II)-exchanged magadiite into Mn-silicalite-1[18,19]. MnMCM-41 produced by the direct hydrothermal and template ion exchange techniques was characterized by Parvulescu[20]. Zhou hypothesized that manganese (II and III) coexisted in the Mn-MCM-41 samples made using different techniques and that a significant portion of Mn species may be integrated to the MCM-41 framework made using the direct hydrothermal technique. The coexistence of manganese cations was examined using electron spin resonance (ESR) and X-ray absorption near edge structure (XANES)[21]. Mn-MCM-41 produced by the DHT technique under mildly alkaline circumstances, framework Mn^{2+} was found[21]. The authors hypothesized that, in addition to the existence of extra-framework Mn^{2+}, thermal treatment in air might cause the convert (oxidation) of Mn^{2+} to Mn^{3+} in the framework structure. Furthermore, It was predicted to result in extra-framework-framework interactions with manganese[21].

Because Mn can be obtained from the starting gel and Al can be replaced by Mn in an isomorphous manner, it was thus obliged to be included in the MFI framework. It was done to synthesize Mn/MFI using various preparations, such as in-situ integration and impregnation techniques. Surface textural examination, FTIR spectroscopy, and X-ray diffraction were employed to describe the sample preparation. Finally, UV-Vis spectroscopy was used to examine the hydroxylation of benzene to phenol in all generated samples.

EXPERIMENTAL

Materials
Sodium hydroxide pellets (AR 98%), Mn $(NO_3)_2$, tetrapropylammonium bromide (TPABr, Fluka), n-propyl amine (n-PA, Merck), rice husk powder RHs (made in this work), and commercial H_2SO_4 were the ingredients employed.

### Silica preparation from rice husk
Cleaning Filtration, air drying, and calcination at 750°C for 6 h (white ash) are the steps that are used to remove any remaining mud and rice particles from rice husk before drying. 12 g of calcined RHs were combined with 150 mL of a 4M NaOH solution and heated at 90°C under reflux for 12 hours. For full precipitation, concentrated hydrochloric acid (20 mL) were added to RHs sample, rinsed in deionized water, filtered and repeated the previous step to remove chloride ions. Finally, the sample was dried at 120°C for 6 hours. Silicalite preparation (MFI) synthesize silicalite-1, the hydrogels with the succeeding oxide molar compositions were formed using the molar ratios:

Na_2O: SiO_2:0:185: 3:12Na_2O: 6:185TPAB:100H_2O
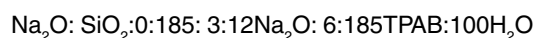
Rice husk-derived silica was mixed with a little amount of water (about 40 mL) and a precise amount of NaOH, then warmed until a transparent solution was obtained at 80°C. In contrast, dissolve templet in little amount of water (10 mL) then heated at 50°C for 20 minutes. The sodium silicate solution received the TPABr solution while being stirred for 15 minutes. As a mobilizing agent, 1 mL of n-propyl amine was applied[22,23]. Using 0.1 M sodium hydroxide and sulphuric acid solutions, the mixture's pH was adjusted to[11]. The mixture was then converted to an oil bath hydrothermal treatment for 8 days at 150°C using autoclaves. At the appointed time, taken out from bath and immediately cooled with cold water. The solid product was filtered and washed with distilled water once the pH of the filtrate dropped to 8. The products were calcined in an air oven for 6 h at 550°C after being dried at 110°C for 10 hours. This sample is marked as MFI.

Preparation of Mn–MFI (built-in)
The following molar ratio description of the synthesis process is given:

SiO_2: 0.185TPABr: 100H_2O: 3:12Na_2O: 0.0138MnO_2: 6.18SiO_2
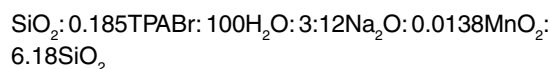
The template tetra propylammonium bromides (TPABr) and the mobilizing agent n-propyl amine were combined with the sodium silicate

solution. While continuously stirring for 30 min, a appropriate amount of manganese nitrate solution was added slowly to the prior solution. adjust the mixture's pH value to 11.0. The amorphous gel was created and aged at room temperature for one hour. The mixture was put into autoclaves and kept there while being heated in an oil bath to 150°C and kept under naturally occurring pressure. The procedure was followed exactly as it was for the sample above, and Mn-MFIin was known as the material.

Mn-loaded MFI by impregnation

Manganese-MFI sample was created by incipient wetness impregnation of MFI (made in this study) with an appropriate amount of Mn $(NO_3)_2$ in an aqueous solution, calculated to provide the necessary percentage of 5wt % MnO_2. The amount of solution required to completely wet the zeolite carrier, along with the slurry's pH of about 6, allowed for this. The reaction temperature was set at 80°C, and the mixture was continually agitated until the extra water evaporated. The precursor was further dried at 120°C over the course of an overnight period, and the decomposition was then conducted in air with a temperature controller of the REX-P 90 type while gradually rising temperature up to 500°C. The preparation was held at this calcination temperature for six hours, during which little Mn was lost.

Instrumental techniques

A Philips diffractometer (PW-3710) was used to measure the X-ray diffractograms of various MFI samples. 30 kV, 10 mA, and a 2θ/min scanning rate, the patterns were operated using Ni-filtered copper radiation (K = 1.5404). The Scherrer equation was used to calculate the prepared materials' crystal sizes. The crystallinity of the samples was calculated as the ratio of the most intense peaks for modified MFI samples (2θ= 20-230) to that of the same peaks for the prepared MFI, and this value was multiplied by 100. The Fourier transform infrared (FTIR) spectra were captured using the Jasco FT-IR-40, a single beam spectrometer with a resolution of 2 cm^{-1}. Two measurements were made at 3800-3000 cm^{-1} and 1400-400 cm^{-1} at room temperature. At-196°C, the nitrogen adsorption isotherms were estimated. The specific surface area was evaluated using the BET method. The exterior surface area and micropore volume were estimated using the t-plot method.

Catalytic activity test

The procedure was carried out in a solvent-free reactor system. The mixture was stirred and heated the catalyst was dried at 383K to separate impurities and water, 50 cm^3 of benzene (Merck, 99.7%), 2 cm^3 of H_2O_2 (30% wt./wt.), and 0.1 g of catalyst were added dropwise to a typical reaction mixture; the reaction took about 30 minutes. To agitate the reaction mixture, a magnetic stirrer was offered. The reaction mixture underwent another 70 minutes of stirring after all the H_2O_2 had been added. After that, the 4-aminoantipyrene method of spectrophotometer was used to detect the concentration of phenol[24,25].

RESULT AND DISCUSSION

XRD

Figure 1 displays the X-ray diffractograms of pure MFI, Mn-MFI$_{in}$, and Mn-MFI$_{imp}$. In silicalite and Mn/MFI$_{imp}$ samples, XRD patterns display a broad line at d=4.2546 and 3.343; this line is indicative of the quartz (Si_3O_6) phase[26,27]. The sample Mn-MFI$_{in}$, on the other hand, did not confirm the presence of quartz silica; hence, the introduction of Mn ions through in-situ preparation methods will cause a rearrangement of the structure of silicalite and disappearance of quartz silica.
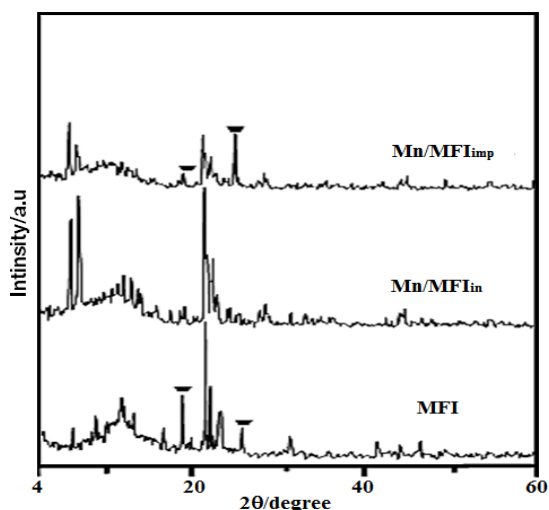

Fig. 1. XRD of the MFI and modified by different methods

Although the presence of MnO_2 species in Mn-MFI$_{imp}$ was not confirmed by comparing the samples before and after the addition of Mn, a little amount of this phase's crystalline

structure is seen in Mn-MFI$_{in}$ at d=5.134 and 1.666. In contrast to these findings, the pattern of Mn/MFI$_{imp}$ revealed a notable overall drop in

diffraction line intensity. The lattice properties and unit cell volume of the samples are summarized in Table 1.

Table 1: Effects of different preparation methods on unit cell characteristics, cell volume, crystallinity, and crystallite size of zeolite samples

Samples	Crystal size (nm)	Unit cell (Å)			Cell Vol.(Å)³	Relative crystallinity%
		a	b	c		
MFI	108	20.105	20.046	13.429	5412	80
Mn-MFI$_{imp}$	119	19.741	20.041	13.421	5309	56
Mn-MFI$_{in}$	135	19.805	20.132	13.712	5467	100

Note: a, b, c is the lattice parameters (Å), V is the lattice volume (Å)3; a*b*c., D is the particles diameter (Å). The crystallinity percentages were obtained by XRD from the sum of the maximum line intensities from 2 : 20-23 Å

Comparing the volume and cell unit characteristics for Mn/MFI$_{imp}$. And Mn/MFI$_{in}$ demonstrated that: i) the Mn ions were deeply induced into the lattice. ii) Partially dealumination may occur during the impregnation method, as shown by the decrease in cell volume in the Mn/MFI$_{imp}$ sample. This is also supported by a significant impact on the entry of Mn ions into samples.

Framework structure

As-prepared MFI, Mn-MFI$_{in}$, and Mn-MFI$_{imp}$ samples' FTIR spectra are depicted in Fig. 2a, the samples' spectra all display a typical MFI structure with modest modifications from the addition of Mn. The bands at 1235 and 1083 cm^{-1} refer to TO$_4$ asymmetric stretching vibration[28-30], whereas the other absorption bands at 796, 550, and 453 cm^{-1} related directly to TO$_4$ symmetric stretching, double ring, and bending vibrations, respectively. The Mn-MFI$_{in}$ IR spectrum exhibits absorption bands at 1229 (1235) and 1085 (1049) cm^{-1} that have been modified to relatively lower wave numbers, indicating good assimilation of Mn species into MFI channels, probably in compensating positions[29].

Importantly, The Mn-MFI$_{in}$ splits into 1120 cm^{-1} in the internal asymmetric stretching vibration of Si-O-T for aluminosilicate (parent MFI), which is found at 1095 cm^{-1} beyond the continued existence of the one at 1049 cm^{-1}. This might be as a result of residual Al^{3+} remaining close Mn^{3+} at the same location. It is logical to correlate a new shoulder at 615 cm^{-1} that was absent in the parent MFI when Mn was added to MFI using different ways with Mn-O vibrations, and more precisely with the lattice vibrations of MII-O bonds[18,31,32]. While it may have been

inherited through MnII-O vibrations, the IR band was particularly important to the XRD observable crystalline structure of MnO$_2$[33].

Crystallinity bands at 450 cm^{-1} (I450) and 550 cm^{-1} (I550) indicates the vibration of TO$_4$ units and five-membered oxygen rings respectively[34–36], the relative crystallinity in the following order: Mn-MFI$_{imp}$< MFI <Mn-MFI$_{in}$, as shown in Table 1 which agrees with the estimate from the XRD analysis.

In Fig. 2b, the IR spectra of the parent MFI zeolite and the Mn-MFI (made using various techniques) are compared in the OH- absorption zone (3800-3400 cm^{-1}). The following bands can be seen in the parent Na-MFI zeolite's spectrum: The lower frequency a broad band at about 3513 cm^{-1} is attributable to hydrogen bound Si-OH species, and the higher frequency a narrow band at about 3747 and 3662 cm^{-1} is due to the O-H stretching vibrations of terminal silanols groups[26,37]. (placed on the exterior surface and weakly acidic). It is possible that silanols with oxygen atoms involved in H-bodings with closer hydroxyls are the cause of the shoulders at 3665 cm^{-1}.

Mn incorporation (Mn-MFIin) causes the band intensity of the terminal Si-OH groups of MFI to increase together with the disappearance of the band at 3665 cm^{-1}. Three new bands simultaneously arise in Mn/ZSM-5 at 3699, 3628, and 3589 cm^{-1}. The former band is representative of OH groups at Mn atoms in non-framework locations, whereas the latter ones reflect acidic hydroxyls of different strengths. This could show the existence of Mn cations in various locations inside ZSM-5 channels[38–40].
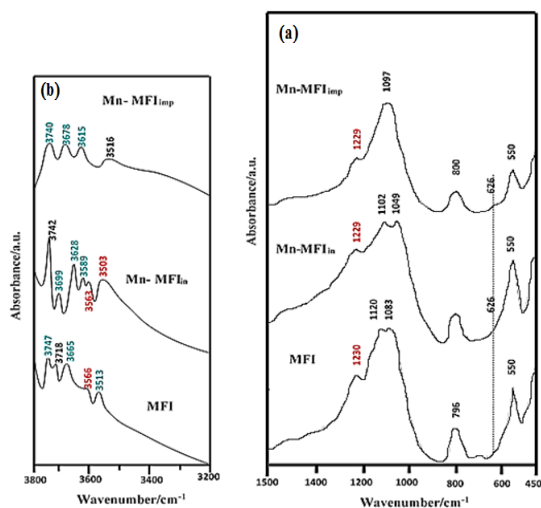
has been expanded to support the requirements for advancing the dealumination process can be found in the Mn-MFI spectrum[41].

Fig. 2: a) FTIR spectra of MFI, Mn-MFlin, and Mn-MFlimp samples b) region of hydroxyl group absorption zone

On the other hand, the Mn-MFI$_{imp}$ sample, when compared to the Mn-MFIin sample, exhibits the same band at 3740, 3678, and 3615 cm^{-1}, but with a lower intensity. A Contrarily, a considerable drop in this band's strength after integration suggests that it does play a role in facilitating the interaction with metal ions. Further evidence that this band's profile

Surface texture

In (Fig. 3 and Table 2), surface texture data were examined and summarized. Examining the data reveals the following information. (i) The in-situ method-prepared sample had the highest specific surface area, whereas Mn-impregnating MFI sample measured the lowest. (ii) The SBET and St values are comparable, showing that the studied solids don't contain ultra-micropores. (iii) The difference of more than 10% between the Sext and the SBET values for the same samples suggests the presence of mesoporosity features. (iv) The mesoporosity of these samples was confirmed by the average pore radius values of comparable materials. (v) In comparison to parallels for as-prepared MFI, the Mn/MFIin samples measured the highest SBET (38%) and Vp^{total} (25%) values. (vi) The Mn/MFI$_{in}$ recorded a greater Vp value compared to the comparable value for other samples, which may be because Mn ions were incorporated in some sites, which reduced the size of wide pores and exposed more microporous features.

Table 2: Surface texture analysis of prepared samples in a particular situation

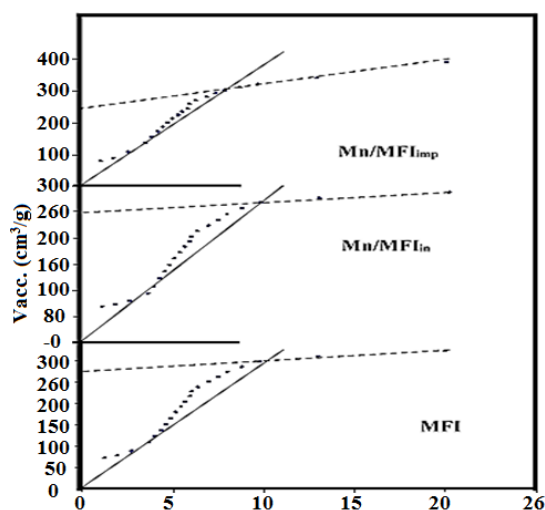| Sample	SBET (m²/g)	St (m²/g)	V_p^{total} (m³/g)	V_p^{μ} (m³/g)	V_p^{wid} (m³/g)	S^{ext} (m²/g)	S^{μ} (m²/g)	S^{wid} (m²/g)	$\bar{r}$ (Å)	Microporosity%
MFI	515	519	0.481	0.430	0.051	36	460	55	24	89
Mn/MFI$_{imp}$	463	456	0.428	0.388	0.040	28	419	44	23	91
Mn/MFI$_{in}$	637	550	0.528	0.393	0.135	105	474	163	21	74

Fig. 3. The surface textures of MFI, Mn-MFlin, and Mn-MFlimp samples

EPR spectroscopy

EPR spectra (Fig. 4) depicts the Mn-MFI$_{in}$ and Mn-MFI$_{imp}$., Zero field transitions were visible in the Mn-MFI$_{in}$. A well-resolved hyperfine sextet typical of MnII was visible in the spectra of as-synthesized Mn-MFI$_{imp}$. EPR spectroscopy can also provide information about MnII integrated into the ZSM-5 lattice. It is widely known that MnII ions randomly orientated in inorganic matrixes where axial symmetry has been imposed exhibit EPR spectra. The outside transitions are not recorded, and the Ms =1/2 -1/2 resonance dominates the spectra[27,42,43]. As previously reported, the MnII/Z X-The band spectrum displays a sharp hyperfine sextet with I = 5/2, S = 5/2 at g=1.9844 and A = 87.5 G. With a tiny zero-field splitting, the primary resonance's location at a g value extremely near to 2 and the observation of well-resolved hyperfine coupling are consistent.
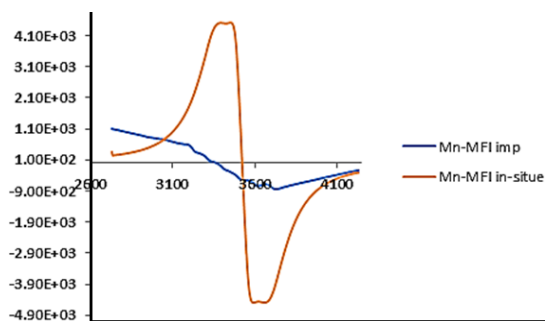
Fig. 4. EPR spectra of Mn-MFIin and Mn-MFIimp

Test reaction

The relative amounts of phenol hydroxylation and H_2O_2 breakdown reactions vary, which contributes to the variance in the activity of the catalysts. Given their ease in switching between two valences, metals with larger redox potentials tend to breakdown H_2O_2 more, Mn (III) converted to Mn (II) have a 1.82V redox potential. This means that Mn-MFI$_{imp}$ > silicalite > Mn-MFI (built-in) would be the expected order of increasing H_2O_2 decomposition activity of the catalysts[44,45].

The ratio of the two reactions' rates will determine the phenol conversions that are seen over the various catalysts: According to observations of the conversion of phenol, the sequence of activity is silicalite> Mn-MFI$_{imp}$> Mn-MFI$_{insitu}$ (built-in). The metal ions that breakdown H_2O_2 quickly (Mn) will be less effective as catalysts for phenol hydroxylation, according to the reverse ordering of

phenol hydroxylation activity and anticipated H_2O_2 decomposition activity. According to the results, silicalite, Mn-MFI$_{imp}$, and Mn-MFI$_{insitu}$ catalysts' catalytic activity and metal ion redox potential are clearly correlated. It is also clear from studies on catalyst concentration that, for silicalite, increasing catalyst concentration from 0.03 to 0.06 g/L significantly reduces phenol hydroxylation. However, the effect was less pronounced for Mn-MFI$_{insitu}$, and for silicalite, the activity is suppressed with increasing catalyst concentration.

CONCLUSION

The process of modification of silicalite with Mn has been successfully carried out using in situ and impregnation techniques. The obtained material was characterized in order to get a full mapping for the surface and entire framework characteristics. Furthermore, the catalytic activity of the obtained material was examined for the hydroxylation of benzene. The data obtained indicate the formation of phenol as a preliminary step of the oxidation process.

ACKNOWLEDGMENT

Conflict of Interest

Author have no conflict of interest.

REFERENCES

1. Sun, Z.; Fridrich, B.; De Santi, A.; Elangovan, S.; Barta, K. *Chem. Rev.*, **2018**, *118*(2), 614–678.
2. Ali, I. O.; El Sayed, H. A.; El-Nasser, K. S.; Shabana, A. A. *J Therm Anal Calorim.,* **2016**, *123*(2), 1129–1139.
3. Ali, I. O.; Hanafy, A. I.; Salama, T. M.; El-Nasser, K. S.; El-Henawy, A. A.; Guma, H. A.; Mohamed, H. M. *Microporous and Mesoporous Materials.*, **2018**, *262*, 35–48.
4. Einaga, H.; Maeda, N.; Teraoka, Y. Applied Catalysis B: *Environmental.*, **2013**, *142*, 406–413.
5. Einaga, H.; Yamamoto, S.; Maeda, N.; Teraoka, Y. *Catalysis Today.*, **2015**, *242*, 287–293.
6. Orazov, M.; Davis, M. E. *Chemical Science.*, **2016**, *7*(3), 2264–2274.
7. Rahmani, N.; Amiri, A.; Ziarani, G. M.; Badiei, A. *Molecular Catalysis.*, **2021**, *515*, 111873.

8. Su, X.; Hu, Z.-P.; Han, J.; Jia, Y.; Xu, S.; Zhang, J.; Fan, D.; Wei, Y.; Liu, Z. *Microporous and Mesoporous Materials.*, **2023**, *348*, 112371.
9. Su, X.; Hu, Z.-P.; Han, J.; Wei, Y.; Liu, Z. *Crystal Growth & Design.*, **2023**, *23*(4), 2644–2651.
10. Domoroshchina, E. N.; Svetogorov, R. D.; Kuz'micheva, G. M.; Kravchenko, G. V.; Pirutko, L. V.; Zhukova, A. I.; Utenyshev, A. N.; Bozhenko, K. V. *J Mater Sci.,* **2023**, *58*(9), 3934–3946.
11. Yabushita, M.; Yoshida, M.; Muto, F.; Horie, M.; Kunitake, Y.; Nishitoba, T.; Maki, S.; Kanie, K.; Yokoi, T.; Muramatsu, A. *Molecular Catalysis.,* **2019**, *478*, 110579.
12. Stadler, B. M.; Wulf, C.; Werner, T.; Tin, S.; De Vries, J. G. *ACS Catal.*, **2019**, *9*(9), 8012–8067.

13. Tsaplin, D. E.; Ostroumova, V. A.; Kulikov, L. A.; Zolotukhina, A. V.; Sadovnikov, A. A.; Kryuchkov, M. D.; Egazaryants, S. V.; Maksimov, A. L.; Wang, K.; Luo, Z. *Catalysts.,* **2023**, *13*(2), 216.

14. Wang, C.; Zhang, J.; Zheng, W.; Ren, Y.; Yue, B.; He, H. In Industrial Arene Chemistry; Mortier, J., Ed.; Wiley, **2023**, 1385–1410.

15. Rahmah, W.; Novita, T. H.; Wenten, I. G.; Kadja, G. T. *Materials Today Sustainability.,* **2023**, 100345.

16. Tao, P.; Wang, X.; Zhao, Q.; Guo, H.; Liu, L.; Qi, X.; Cui, W. *Applied Catalysis B: Environmental* **2023**, *325*, 122392.

17. Zhu, C.; Huang, C.; Zhang, M.; Fang, K. *Fuel.,* **2023**, *335*, 126745.

18. Tušar, N. N.; Logar, N. Z.; Ar on, I.; Thibault-Starzyk, F.; Risti , A.; Raji , N.; Kau i , V. *Chem. Mater.*, **2003**, *15*(25), 4745–4750.

19. Zhao, J.; Zhang, Y.; Zhang, S.; Wang, Q.; Chen, M.; Hu, T.; Meng, C. *Microporous and Mesoporous Materials.,* **2018**, *268*, 16–24.

20. Parvulescu, V. In Redox; Intech Open, **2019**.

21. Zhou, S.; Yang, F.; Wang, B.; Su, H.; Lu, K.; Ding, Y.; Lei, K.; Xu, M.; Shao, B.; Wang, Y. *Catalysts.,* **2018**, *8*(2), 80.

22. Salam, M. A.; Ahmed, K.; Hossain, T.; Habib, M. S.; Uddin, M. S.; Papri, N. International *Journal Of Chemistry, Mathematics And Physics (IJCMP).,* **2019**, *3*(6).

23. Khaleque, A.; Alam, M. M.; Hoque, M.; Mondal, S.; Haider, J. B.; Xu, B.; Johir, M. A. H.; Karmakar, A. K.; Zhou, J. L.; Ahmed, M. B. Environmental Advances 2020, 2, 100019.

24. Zeng, Z.; Tian, L.; Li, Z.; Jia, L.; Zhang, X.; Xia, M.; Hu, Y. *Biosensors and Bioelectronics.,* **2015**, *69*, 162–166.

25. Fernando, C. D.; Soysa, P. *Methods X.,* **2015**, *2*, 283–291.

26. Sun, Z.; Yan, Y.; Li, G.; Zhang, Y.; Tang, Y. *Ind. Eng. Chem. Res.*, **2017**, *56*(39), 11167–11174.

27. Patra, A. K.; Dutta, A.; Pramanik, M.; Nandi, M.; Uyama, H.; Bhaumik, A. *Chem. Cat. Chem.,* **2014**, *6*(1), 220–229.

28. Wang, Y.; Jia, H.; Fang, X.; Qiu, Z.; Du, T. *RSC advances.*, **2020**, *10*(41), 24642–24652.

29. Meng, Y.; Genuino, H. C.; Kuo, C.-H.; Huang, H.; Chen, S.-Y.; Zhang, L.; Rossi, A.; Suib, S. L. *J. Am. Chem. Soc.*, **2013**, *135*(23), 8594–8605.

30. Zhang, Y.; Yu, Q.; Tang, X.; Zhao, S.; Gao, F.;

Yuan, Y.; Zhang, J.; Wei, J.; Yi, H. *Separation and Purification Technology.,* **2022**, *300*, 121687.

31. Rac, V.; Raki , V.; Damjanovi -Vasili , L.; Dondur, V.; Auroux, A. *Applied Surface Science.*, **2017**, *423*, 1134–1140.

32. Baran, R.; Valentin, L.; Dzwigaj, S. *Physical Chemistry Chemical Physics.,* **2016**, *18*(17), 12050–12057.

33. Dinh, V.-P.; Luu, T. A.; Siemek, K.; Kozlenko, D. P.; Le, K. H.; Dang, N. T.; Nguyen, T. V.; Le Phuc, N.; Tran, T. D.; Phan, P. T.; Lo, S. T.; Hoang, K. A. T.; Dinh, T. K.; Luong, N. T.; Le, N. C.; Nguyen, N.-T.; Ho, T.-H.; Tran, X. D.; Tran, P. D.; Nguyen, H. Q. *Langmuir.,* **2022**, *38*(50), 15604–15613.

34. Pop, O. L.; Diaconeasa, Z.; Mesaro , A.; Vodnar, D. C.; Cuibus, L.; Ciontea, L.; Socaciu, C. *Bulletin UASVM Food Science and Technology.,* **2015**, *72*(1), 50–55.

35. Meng, Y.; Genuino, H. C.; Kuo, C.-H.; Huang, H.; Chen, S.-Y.; Zhang, L.; Rossi, A.; Suib, S. L. *J. Am. Chem. Soc.*, **2013**, *135*(23), 8594–8605.

36. Razavian, M.; Fatemi, S.; Komasi, M. *Materials Research Bulletin.,* **2015**, *65*, 253–259.

37. Koshti, H.; Bandyopadhyay, M.; Bandyopadhyay, R. *J Mater Sci.,* **2023**, *58*(29), 11914–11936.

38. Zhang, P.; Yang, X.; Hou, X.; Mi, J.; Yuan, Z.; Huang, J.; Stampfl, C. *Catalysis Science & Technology.,* **2019**, *9*(22), 6297–6307.

39. Ben Younes, N.; Ortigosa, J. M.; Marie, O.; Blasco, T.; Mhamdi, M. *Res Chem Intermed.,* **2021**, *47*(5), 2003–2028.

40. Kamaluddin, H. S.; Gong, X.; Ma, P.; Narasimharao, K.; Chowdhury, A. D.; Mokhtar, M. *Materials Today Chemistry.,* **2022**, *26*, 101061.

41. Dubray, F. PhD Thesis, Normandie Université, **2020**.

42. Montejo-Valencia, B. D.; Pagán-Torres, Y. J.; Martínez-Iñesta, M. M.; Curet-Arana, M. C. *ACS Catal.*, **2017**, *7*(10), 6719–6728.

43. Ali, I. O.; Hanafy, A. I.; Salama, T. M.; El-Nasser, K. S.; El Henawy, A. A.; Guma, H. A.; Mohamed, H. M. *Microporous and Mesoporous Materials.,* **2018**, *262*, 35–48.

44. Gao, Y.; Pan, Z.; Sun, J.; Liu, Z.; Wang, *J. Nano-Micro Lett.,* **2022**, *14*(1), 94. (45)

45. Li, C.; Han, X.; Cheng, F.; Hu, Y.; Chen, C.; Chen, *J. Nature communications.,* **2015**, *6*(1), 7345.